Interaction of Rare Earth Elements and Graphite Coated with Yttrium Oxide

HyunWoo Seong[a] , Seoung Woo Kuk [b] , SangHun Lee [b] , Ho Jin Ryu [a*],
[a] *Department of Nuclear & Quantum Engineering, Korea Advanced Institute of Science and Technology, 291 Daehakro, Yuseong, 34141, Republic of Korea*
[b] *Korea Atomic Energy Research Institute, Daedeok-daero 989-111, Yuseong-gu, Daejeon, 34057, Republic of Korea*
[*] *Corresponding author: hojinryu@kaist.ac.kr*

1. Introduction

Metallic fuels have many advantages such as a high density of fissile and fertile materials, a high thermal conductivity, a high breeding performance, a simple fabrication procedure, and a good compatibility with sodium coolant. So, metallic fuels are ideal for sodium-cooled fast reactor (SFR) fuels. Especially uranium-zirconium (U-Zr) and uranium-zirconium-plutonium (U-Zr-Pu) alloys are considered as excellent metallic fuels because of the high melting point, reliable fuel swelling, and reliable fuel performance [1–5]. In Korea, resource of metallic fuels is obtained by using pyroprocessing of pressurized water reactor (PWR) spent nuclear fuels. In spent nuclear fuels, there are many fission product elements. Rare earth elements (REEs) such as lanthanum (La), cerium (Ce), praseodymium (Pr), and neodymium (Nd) is one of the fission product elements. Since the chemical properties of REEs and trans-uranium element (TRU) are similar, separation of REEs and TRU by using pyro-processing is difficult [6,7]. Therefore, it is high cost to keep the REEs component at a lower concentration in the metallic fuels. There are several fabrication methods of fuels. Injection casting is one of the fabrication methods of metallic fuels with advantages in terms of fabricating small-diameter casting with a high L/D ratio and a randomly oriented grain structure [8–11]. In injection casting, metallic fuel pins have been remotely fabricated using a quartz mold assembly and graphite crucible. Since uranium metal is very reactive with crucible or mold materials such as graphite and quartz, graphite crucible and quartz coated with yttrium oxide were used to prevent carbon contamination from the crucible to metallic fuels. The yttrium oxide coating is made by a plasma spray process. However, a deficiency of REEs occurs in the molten metals during injection casting. One of the reason is that there are some interactions between REEs and yttrium oxide coating [12].

This paper discusses the microstructure of the interface of REEs and graphite coated with yttrium oxide. The main objective is to observe the interaction of REEs and yttria in a high-temperature environment. If the reaction occurs with rare earth and yttrium oxide, then the products may be useful in improving the stability of the coating on graphite mold.

2. Experimental procedures

The REEs alloys were fabricated using four different lanthanide elements; Nd, Ce, Pr, and La with an overall composition of 53, 25, 16 and 6 wt.%, respectively. The composition of this REEs was set according to the expected conditions of REEs in the TRU ingot after the pyroprocessing of the PWR spent fuel [13]. The graphite sample was coated with yttria using a high temperature plasma spray coating. The size of graphite coated with yttria sample is 20 mm in diameter and 5 mm in thickness. REEs alloy about 0.5 g was polished using a SiC abrasive wheel, to remove the oxide layer before putting in the box furnace. Heating REEs alloy and graphite coated with yttria was performed using a box furnace (S-1700, HanTech). REEs alloy was placed on the graphite coated with yttria and put into the box furnace. The process conditions of the box furnace are to raise the temperature to 1500 °C by 10 °C/1min, maintain it for 10 minutes, and then cool down. Ar gas was injected into the box furnace at 5 l/min to prevent oxidation of the REEs alloy (**Fig.1**). After the process the sample was encapsulated by epoxy resin to prevent oxidation of the REEs alloy. The sample was cut perpendicularly using diamond cutting and was polished using a SiC abrasive wheel.
Microstructures of the interface of REEs alloy and yttria were observed by using back scattered electron (BSE) mode in scanning electron microscopy (SEM) (CX-200TM, COXEM). Their elemental distributions were observed by using energy-dispersive X-ray spectroscopy (EDS) (CX-200TM, COXEM). And the qualitative analysis of the sample was identified by using X-ray diffraction analysis (XRD) (Smartlab, RIGAKU) with Cu $K_{\alpha 1}$ radiation (λ=0.15406 nm) in θ-2θ configuration at a 2°/min for scan speed and 0.01° for step size.

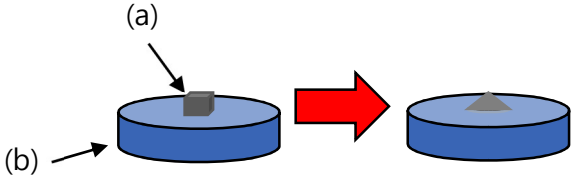

Fig. 1. Schematic of the experiment. A red arrow means heating in a box furnace. (a) is REEs alloy. (b) is graphite coated with yttria.

3. Results and discussion

3.1 Microstructure and Chemical composition

The perpendicularly cross-sectional SEM-BSE image of REEs alloy and graphite coated with yttria is shown in **Fig. 2**. When zoom in the top and middle of REEs alloy portions, there are two regions in top and middle of REEs alloy; dark gray and gray regions (**Fig.3**). The compositions of the dark gray and gray regions are presented in **Table I** for seven different elements; Nd, Ce, Pr, La, Y, O, and Si, obtained via EDS analysis. The gray regions consisted of very small Y, which can be regarded as an error range. So, the gray regions can be seen as a matrix. It can be seen that the dark gray regions consisted of not only REEs but also Y and O. It means that there is some interaction of REEs and yttria. The melting temperatures of Nd, Ce, Pr and La are 1,024 °C, 795 °C, 935 °C, and 920 °C, respectively, while the melting temperature of Y_2O_3 is 2425 °C. Since the process temperature rises to 1500 °C, the REEs alloy dissolves but the yttria doesn't dissolve. Moreover, the densities of Nd, Ce, Pr, La, and Y_2O_3 are 7.01, 6.77, 6.77, 6.16, and 5.01 g/cm^3, respectively. When REEs alloy reacts with yttria to form products, they float on REEs alloy because of the lower density than REEs alloy. Therefore, the dark gray regions of the top of REEs alloy contains more Y than the dark gray regions of the middle of REEs alloy. The Si component is detected inside the REEs alloy, which seems to be Si buried while using the SiC abrasive. The SEM-BSE image of the interface of REEs and graphite coated with yttria is shown in **Fig.4**(a). In order to analyze it in detail, three parts of Fig.4(a) were zoomed in (**Fig.4**(b)-(d)). REEs were detected at yttria region. Also, the composition ratio of Nd, Ce, Pr, and La were changed compared with the initial composition ratio (53, 25, 16 and 6 wt.%, respectively) (**Fig.5**). It means that reactions have occurred with some elements of REEs and yttria, but it was difficult to demonstrate exactly what elements reacted and why occurred in this paper. There are two regions in yttria portion; dark gray

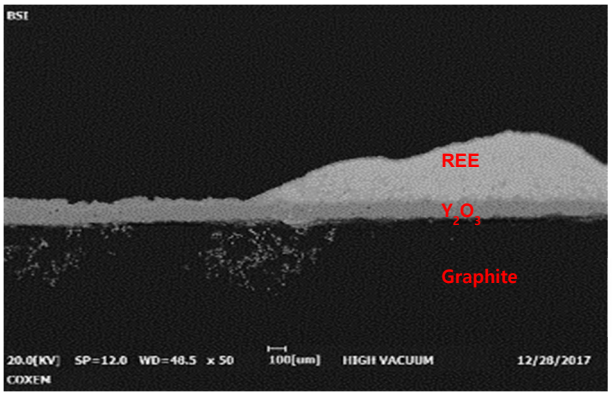

Fig. 2. The cross-sectional SEM-BSE image of REEs alloy and graphite coated with yttria.

Table I: Element composition of the Fig.3.

	Element composition (wt.% , at.%)						
	Nd	*Ce*	*Pr*	*LA*	*Y*	*O*	*Si*
#1	43.1	6.4	7.9	1.1	16.8	24.7	-
	14.0	2.2	2.6	0.4	8.8	72.0	-
#2	32.1	6.4	6.3	0.6	14.2	40.4	-
	7.4	1.5	1.5	0.2	5.3	84.1	-
#3	36.5	7.0	6.1	1.4	12.5	36.5	-
	9.1	1.8	1.5	0.4	5.1	82.1	-
#4	37.9	7.1	7.1	1.1	15.0	31.8	-
	10.4	2.0	2.0	0.3	6.7	78.6	-
#5	48.9	8.8	8.1	1.1	6.2	26.9	-
	15.3	2.8	2.6	0.4	3.1	75.8	-
#6	50.4	26.9	15.9	5.6	0.2	1.0	-
	46.0	25.3	14.9	5.2	0.3	8.3	-
#7	50.4	18.2	14.3	2.0	1.4	4.7	9.0
	28.6	10.6	8.3	1.2	1.3	23.9	26.1
#8	46.4	24.3	13.8	3.7	1.8	3.4	6.6
	29.5	16.0	9.0	2.4	1.8	19.8	21.5
#9	45.2	21.8	14.2	5.1	1.5	12.2	-
	22.7	11.2	7.3	2.7	1.2	54.9	-
#10	47.0	22.0	15.1	5.8	0.0	10.1	-
	25.8	12.4	8.5	3.3	0.0	50.0	-

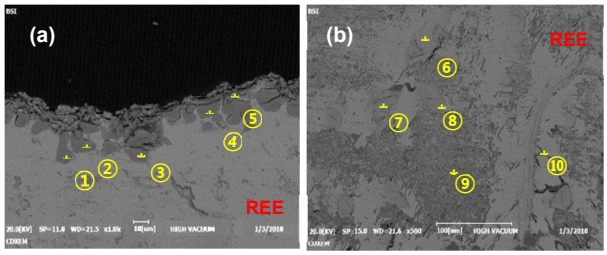

Fig. 3. SEM-BSE image to analyze point-scanning images. (a) is top of REE alloy. (b) is middle of REE alloy.

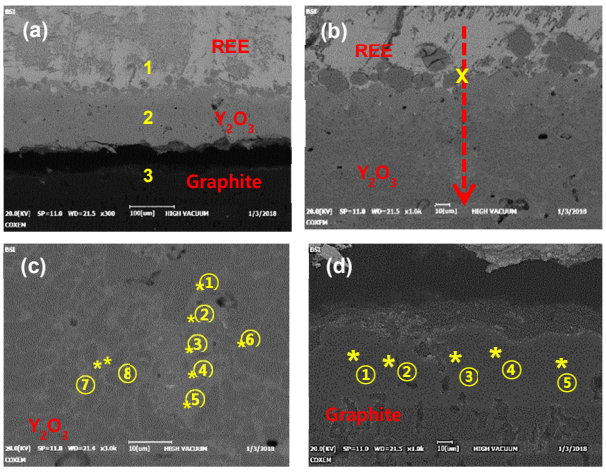

Fig. 4. (a) is an SEM-BSE image of the interface of REEs and graphite coated with yttria. (b) is a line-scanning image of the interface of REEs and yttria, (c) is a point-scanning image of yttria, and (d) is a point-scanning image of graphite.

Table II: Element composition of Fig.4 (c)

	Element composition (wt.% , at.%)					
	Nd	*Ce*	*Pr*	*LA*	*Y*	*O*
#1	0.7	0.1	0.2	0.3	74.8	23.9
	0.2	0.0	0.1	0.1	35.9	63.8
#2	1.1	0.7	0.3	0.2	73.5	24.2
	0.3	0.2	0.1	0.1	35.1	64.2
#3	16.6	5.3	3.8	1.3	53.3	19.7
	5.7	1.9	1.3	0.4	29.7	61.0
#4	19.8	6.9	4.8	1.7	47.5	19.3
	7.0	2.5	1.7	0.6	27.1	61.1
#5	23.3	10.7	6.1	3.0	40.4	16.5
	9.1	4.3	2.4	1.2	25.4	57.6
#6	1.2	0.6	0.4	0.2	75.1	22.5
	0.4	0.2	0.1	0.1	37.3	61.9
#7	2.4	0.7	0.4	0.3	72.1	24.1
	0.7	0.2	0.1	0.1	34.6	64.3
#8	19.5	3.4	4.2	0.8	54.7	17.4
	7.1	1.3	1.5	0.3	32.4	57.4

Table III: Element composition of Fig.4 (d)

	Element composition (wt.% , at.%)						
	C	*Nd*	*Ce*	*Pr*	*LA*	*Y*	*O*
#1	93.9	0.2	0.1	0.1	0.2	0.4	5.1
	96.0	0.0	0.0	0.0	0.0	0.1	3.9
#2	92.5	0.3	0.1	0.2	0.2	0.6	6.1
	95.1	0.0	0.0	0.0	0.0	0.1	4.8
#3	84.8	0.3	0.1	0.0	0.0	0.8	14.0
	88.8	0.0	0.0	0.0	0.0	0.1	11.1
#4	94.3	0.3	0.2	0.1	0.1	0.4	4.6
	96.4	0.0	0.0	0.0	0.0	0.1	3.5
#5	92.9	0.1	0.3	0.1	0.1	0.5	6.0
	95.3	0.0	0.0	0.0	0.0	0.1	4.6

and gray regions (**Fig.4**(c)). The dark gray regions consisted of very small REEs, which can be regarded as an error range. Dark gray regions can be seen as a matrix. It can be seen that the gray regions consisted of not only Y and O but also REEs (**Table II**). It means that REEs can penetrate into the yttria. Graphite portion consisted of very small REEs and Y, which can be regarded as an error range (**Table III**). Therefore, REEs and Y don't penetrate into the graphite region.

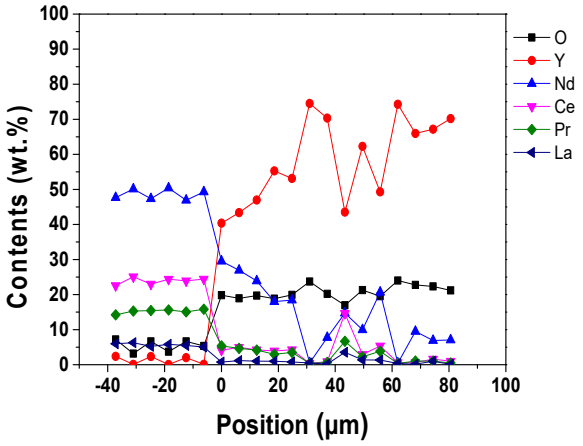

Fig. 5. Distribution data of REEs, Y, and O contents on the interface of REEs and yttria.

3.2 X-ray diffraction (XRD) analysis

Fig. 6. shows XRD 2θ pattern of the interface of REEs and yttria. There are many peaks. Because of similar chemical properties of lanthanide, peaks overlap. Therefore, it is not known exactly which peak corresponds to which substance. However, it is clear that there are other peaks not peaks of REEs, REEs oxide, yttria. Candidates of the peaks are $Pr_{1.2}Y_{0.8}O_{3.6}$, $Ce_{0.5}La_{0.5}YO_{3.25}$, $YPrO_3$, $Ce_{0.87}Y_{0.13}$, and so on. To analyze exactly, the experiment should be proceeded as each REE instead of the REEs alloy because of peaks overlap.

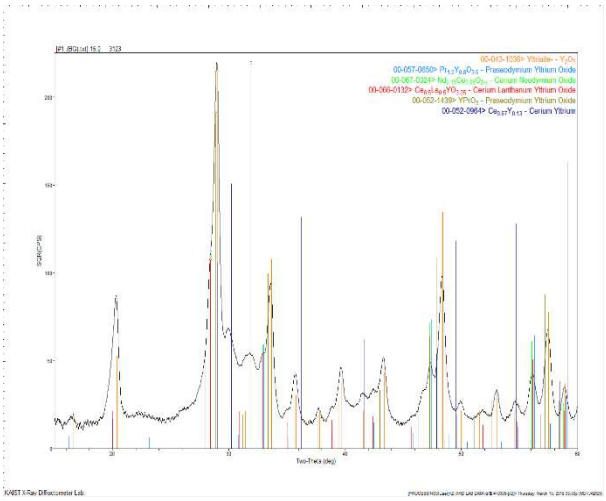

Fig. 6. X-ray diffraction patterns of gas-atomized and cryomilled powder

4. Conclusion

The REEs alloys and graphite coated with yttria using a high temperature plasma spray were fabricated, put in high temperature environment and analyzed. The present research has resulted in the following conclusions:

1. Rare earth elements react with yttrium oxide and form complex reaction products at high temperature.
2. Rare earth elements did not penetrate into the graphite region.

ACKNOWLEDGMENT

This study was supported by KAERI (NRF-2017M2A8A5018431)

REFERENCES

[1] G. L. HOFMAN et.al, Metallci Fast Reactor Fuels, Prog. Nucl. Energy. 31 (1997) 83–110.

[2] J.H. Kittel, B.R.T. Frost, J.P. Mustelier, K.Q. Bagley, G.C. Crittenden, J. Van Dievoet, History of fast reactor fuel development, J. Nucl. Mater. 204 (1993) 1–13. doi:10.1016/0022-3115(93)90193-3.

[3] D.C. Crawford, D.L. Porter, S.L. Hayes, Fuels for sodium-cooled fast reactors: US perspective, J. Nucl. Mater. 371 (2007) 202–231. doi:10.1016/j.jnucmat.2007.05.010.

[4] L.C. Walters, Thirty years of fuels and materials information from EBR-II, J. Nucl. Mater. 270 (1999) 39–48. doi:10.1016/S0022-3115(98)00760-0.

[5] M. Akabori, A. Itoh, T. Ogawa, F. Kobayashi, Y. Suzuki, Stability and structure of the δ phase of the U-Zr alloys, J. Nucl. Mater. 188 (1992) 249–254. doi:10.1016/0022-3115(92)90480-9.

[6] M. Sakata, M. Kurata, T. Hijikata, T. Inoue, Equilibrium distribution of rare earth elements between molten KCl-LiCl eutectic salt and liquid cadmium, J. Nucl. Mater. 185 (1991) 56–65. doi:10.1016/0022-3115(91)90365-E.

[7] K. Uozumi, Y. Sakamura, K. Kinoshita, T. Hijikata, T. Inoue, T. Koyama, Development of pyropartitioning process to recover minor actinide elements from high level liquid waste, Energy Procedia. 7 (2011) 437–443. doi:10.1016/j.egypro.2011.06.058.

[8] J.H. Kim, H. Song, K.H. Kim, C.B. Lee, Fabrication and evaluation of rare-earth-bearing fuel slugs for sodium-cooled fast reactors, J. Radioanal. Nucl. Chem. 303 (2015) 615–621. doi:10.1007/s10967-014-3513-3.

[9] J.H. Kim, H. Song, K.H. Kim, C.B. Lee, Fabrication of uranium alloy fuel slug for sodium-cooled fast reactor by injection casting, J. Radioanal. Nucl. Chem. 301 (2014) 797–803. doi:10.1007/s10967-014-3202-2.

[10] C.L. Trybus, J.E. Sanecki, S.P. Henslee, Casting of metallic fuel containing minor actinide additions, J. Nucl. Mater. 204 (1993) 50–55. doi:10.1016/0022-3115(93)90198-8.

[11] D.E. Burkes, R.S. Fielding, D.L. Porter, D.C. Crawford, M.K. Meyer, A US perspective on fast reactor fuel fabrication technology and experience part I: metal fuels and assembly design, J. Nucl. Mater. 389 (2009) 458–469. doi:10.1016/j.jnucmat.2009.02.035.

[12] S.W. Kuk, K.H. Kim, J.H. Kim, H. Song, S.J. Oh, J.Y. Park, C.B. Lee, Y.S. Youn, J.Y. Kim, Phase characteristics of rare earth elements in metallic fuel for a sodium-cooled fast reactor by injection casting, J. Nucl. Mater. 486 (2017) 53–59. doi:10.1016/j.jnucmat.2017.01.018.

[13] H.J. Maclean, S.L. Hayes, Irradiation of Metallic and Oxide Fuels for Actinide Transmutation in the ATR, Ratio. (2012) 1341–1345.